Journal of Photochemistry and Photobiology A: Chemistry 209 (2010) 19–26

Contents lists available at ScienceDirect

Journal of Photochemistry and Photobiology A: Chemistry

journal homepage: www.elsevier.com/locate/jphotochem

Theoretical and experimental study of the vertical excitation energies in the ionic and tautomeric forms of 4-aminomethylpyridine

Miquel Adrover, Juan Frau, Catalina Caldés, Bartolomé Vilanova, Josefa Donoso, Francisco Muñoz*

Institut Universitari d'Investigació en Ciències de la Salut (IUNICS), Departament de Química, Universitat de les Illes Balears, Ctra. Valldemossa km 7.5, E-07122 Palma de Mallorca, Spain

ARTICLE INFO

Article history:
Received 23 July 2009
Received in revised form
24 September 2009
Accepted 3 October 2009
Available online 13 October 2009

Keywords:
Time-dependent density functional theory
DFT calculations
4-Aminomethylpyridine
Deconvolution of UV–vis spectra
Structural and electronic properties

ABSTRACT

4-Aminomethylpyridine (4-PAM) has been widely used as a model compound to elucidate the mechanisms of biological and biomedical action of the amino derivatives of vitamin B_6. By virtue of the presence of two ionizable groups (*viz.* a pyridine nitrogen and an amino function) in its structure, 4-PAM in solution occurs as various ionic and tautomeric forms in equilibrium. In this work, we optimized the geometries of such forms and found the protonation status of the ionizable groups in 4-PAM to affect the molecular geometry and frontier orbitals. In addition, we determined the experimental electronic excitation energies for each molecular species of 4-PAM from deconvoluted UV–vis spectra. The results thus obtained were compared with their theoretical counterparts as determined from TD-DFT calculations. Based on the outcome, the theoretical methodology used affords correct simulation of electronic excitation energies. The theoretical and experimental results showed that the deprotonation of the pyridine nitrogen has no effect on the energy of the first electronic transition, however it affects its intensity. Additionally, the deprotonation of both pyridine nitrogen and methylamino group increases the number of bands, by increasing the n–π^* transitions.

1. Introduction

A sound knowledge of molecular electronic functions in ground and excited electronic states is crucial with a view to determining a number of physico-chemical – particularly spectroscopic and photochemical – properties of some molecules. Theoretical computation methods have been widely used for this purpose, and also for the simulation and prediction of such properties.

Geometries, energies in excited electronic states, and UV–vis spectra were originally simulated by using the semi-empirical method ZINDO in combination with configuration interaction as applied to electronic excitation (the CIS method) [1–3]. Subsequently, a combination of the CIS method and Hartree–Fock calculations (the HF–CIS method) facilitated more accurate simulation of energies and geometries for excited states [4–6]. At present, the CASPT2 method (complete active space with second-order perturbation) and its multistate variant (MS-CASPT2) are very good methods for calculating electronic excitation energies [7–9]. Recently, the EOM-CC method (equation-of-motion coupled cluster) has emerged as a powerful tool in this kind of calculations [10]. However, due to the high computational cost the application of these methods is limited to systems with only few electrons.

The time-dependent generalization of the density functional theory (TD-DFT) [11] also provides an accurate choice for calculating excitation energies in both organic and inorganic compounds [12,13]. The results obtained with this methodology are quite consistent with experimental values [11] and more accurate than those provided by the time-dependent generalization of the HF method (TD–HF) [14,15] and the HF–CIS method [4,16]. Today, TD-DFT methods are an attractive alternative to the high computational cost methods [17,18]. However, the accuracy of TD-DFT calculations has been found to rely strongly on the choice of an appropriate functional [6,19,20].

The previous computational techniques have been successfully used to study model aromatic compounds and other molecules of chemical and/or biological interest [21–24]. Thus, they have enabled the study of excited electronic states in monosubstituted benzenes [25], the intramolecular proton transfer in the excited states of salicylic acid and its analogues [26], the simulation of UV–vis spectra for substituted phenols [27] and the calculation of pK_a for their excited states [28].

The presence of a pyridine ring in some biologically interesting compounds (vitamins B_3 and B_6, NAD^+) and drugs (nifedipine, piroxicam) has led to their use as model compounds of special interest. Thus, Cai and Reimers [29,30] examined the electronic excitation energies of pyridine and the effect of excitation on its molecular geometry. Lorenc et al. [31,32] expanded their work by simulating the excitation energies of 4-nitropyridines and exam-

* Corresponding author. Tel.: +34 971 173252; fax: +34 971 173426.
E-mail address: dqufmi0@uib.es (F. Muñoz).

1010-6030/$ – see front matter © 2009 Elsevier B.V. All rights reserved.
doi:10.1016/j.jphotochem.2009.10.003

ined the effect of solvent polarity on their electronic excitation. Some authors have simulated the UV–vis spectra for 2-hydroxy-5-substituted pyridine radicals [33]. Finally, our group simulated the excitation energies for the molecular species of pyridoxamine 5′-phosphate by using semi-empirical methodology [34].

Pyridoxamine, which is the amino derivative of vitamin B_6, possesses a high biological and biomedical significance. Thus, it takes part in the enzymatic transamination of aminoacids [35] and is thought to be a powerful inhibitor of protein glycation [36]. Its structure possesses three ionizable groups that lead to the establishment of a number of equilibria between its ionic and tautomeric forms. The simultaneous presence of such forms has so far precluded their physico-chemical characterization, which is essential with a view to properly understanding the mechanisms of biological and biomedical action of pyridoxamine. One of the most widely used techniques for studying its ionic and tautomeric equilibria is based on deconvolution of its UV–vis spectra into log–normal bands. This has allowed the energy of the first π–π^* transition in each tautomer, and the corresponding band parameters, to be estimated [37,38]. Also, it has enabled an accurate description of the ionization equilibria of pyridoxamine [37], other B_6 vitamins [39,40] and the Schiff bases of pyridoxal 5′-phosphate [41–43].

However, some bands in the characteristic spectrum for each pyridoxamine tautomer remain unassigned. Also, the effect of the protonation status of each ionizable group on electron excitation and other molecular and electronic properties is unknown. The structural complexity of pyridoxamine has so far hindered a thorough description. This led us to study a structurally simpler model compound (*viz.* 4-aminomethylpyridine, 4-PAM) in this work (see Scheme 1). 4-PAM consists of a pyridine ring bearing a methylamino group at position 4; as a result, it only exhibits two ionic equilibria and a single tautomeric equilibrium in solution. By virtue of its similarity to pyridoxamine, 4-PAM was previously used to elucidate the mechanism of action of the former on the transamination of aminoacids [44] and inhibition of protein glycation [45,46].

In this work, we determined the UV–vis spectra of the 4-PAM species (P, HP^+ and H_2P^{2+}, see Scheme 1) and deconvoluted them into different electronic transitions, represented by log–normal curves. Additionally, PCM-TD-DFT calculations of the different species with two salvation water molecules were carried out in order to rationalize the electronic transitions of 4-PAM species.

2. Methodology

2.1. Experimental details

2.1.1. Materials

4-Aminomethylpyridine, succinic acid, boric acid and D_2O were purchased from Sigma–Aldrich. Hydrochloric acid, sodium chloroacetate, sodium acetate, potassium dihydrogen phosphate, potassium bicarbonate, potassium chloride and sodium hydroxide were supplied by Scharlab, S.L. All reagents were used as received. Buffer solutions were made from reagent-grade chemicals and Milli-Q water was used throughout.

2.1.2. UV–vis spectra

Absorption spectra were recorded at 25 ± 0.1 °C on a Shimadzu UV-2401 PC double-beam spectrophotometer. Quartz cells of 1 cm path length were used to obtain electronic spectra. Spectroscopic data were acquired over the energy range from 3.10 eV (400 nm) to 5.90 eV (210 nm). The buffer solution background spectrum was used as spectral reference. UV–vis spectra were obtained in various 0.02 M buffers having an ionic strength of 0.1 M adjusted by addition of KCl as required. The reagents used to prepare the buffer solutions were HCl (pH 1), sodium chloroacetate (pH 2 and 3), sodium acetate (pH 4 and 5), succinic acid (pH 6), potassium dihydrogen phosphate (pH 7, 7.5 and 8), boric acid (pH 8.5 and 9), potassium bicarbonate (pH 10 and 11) and NaOH (pH 12 and 13). Each buffer was used to prepare a solution containing 0.3 mM 4-PAM.

2.1.3. Analysis of UV–vis spectra

The 15 individual UV–vis spectra obtained at each pH were used as inputs for the factor analysis software SPECFIT/32™ [47]. This software performs a global analysis of equilibrium systems with singular value decomposition and non-linear regression. Based on an equilibrium scheme between the different ionic forms, the software analyses mixed pH-dependent spectra and splits them into an individual spectrum for each ionic species in equilibrium. In addition, the fitting procedure allows one to determine the dissociation constants for the equilibrium scheme concerned.

2.1.4. Band deconvolution analysis

Electronic transitions reflected in the presence of individual bands in the UV–vis spectrum for 4-PAM. Such bands were described in terms of four parameters, namely: position (excitation energy, E_{exc}), intensity (molar absorption coefficient, ε; oscillator strength, f), width (W) and asymmetry (ρ). These bands were obtained from UV–vis spectra deconvolution by fitting the obtained spectra to a sum of 2–4 log–normal functions to resolve the contribution of the each individual band to the overall absorption. Log–normal curves, which exhibit some asymmetry ($\rho > 1$), fit the UV–vis spectral profiles for pyridine compounds quite closely [37–43,48] and have been widely used for spectral deconvolution [37–43,49–51]. Our curves were fitted by using the commercial software PeakFit v. 4.0 [52]. The input data consisted of an initial set of parameter estimated for each peak which the software iteratively optimized by reducing the difference between the experimental values and the combined curve obtained from the initial log–normal curve estimates.

2.1.5. NMR spectra

The ^{13}C NMR spectra for 4-PAM were recorded at room temperature on a Bruker AMX-300 spectrometer, using sample tubes 5 mm in diameter and 3-(trimethylsilyl)-1-propanesulphonic acid (DSS) as internal standard. Solutions containing 20 mM 4-PAM in a buffer consisting of either 0.1 M HCl (pH 1), 0.5 M phosphate (pH 6.5) or 0.1 M NaOH (pH 13), all in an 80:20 H_2O-buffer/D_2O ratio, were used for this purpose.

2.2. Computational details

The ground state (S_0) of each 4-PAM form (see Scheme 1) with two water molecules solvating nitrogen atoms was optimized at the Hartree–Fock (HF) and second-order Moller–Plesset perturbation (MP2) [53] theory levels. Both were used in combination with the 6-311++G** basis set. Inclusion of polarization functions in this type of calculation may increase the accuracy of predictions for hydrogen bonds [12]. We processed the first two predicted singlet excited states (S_1 and S_2) for the excited state expansions of 4-PAM forms. Optimized excited state energies and geometries were determined by using the configuration interaction with single excitations (CIS) procedure [54] in conjunction with the 6-311++G** basis set. CIS describes the excited state wave function at a level comparable to HF by using single excitations from the HF determinant. However, the transition wavelengths it provides are quite different from the experimental values [4,16]. In order to simulate the effects of the polar solvent, the polarizable continuum model (PCM) was used [55]. The solvent used for all calculations was water (ε = 78.4).

Excited state oscillator strengths (f) and the excitation energy (E_{exc}) for each 4-PAM form were obtained in a single-point calcu-

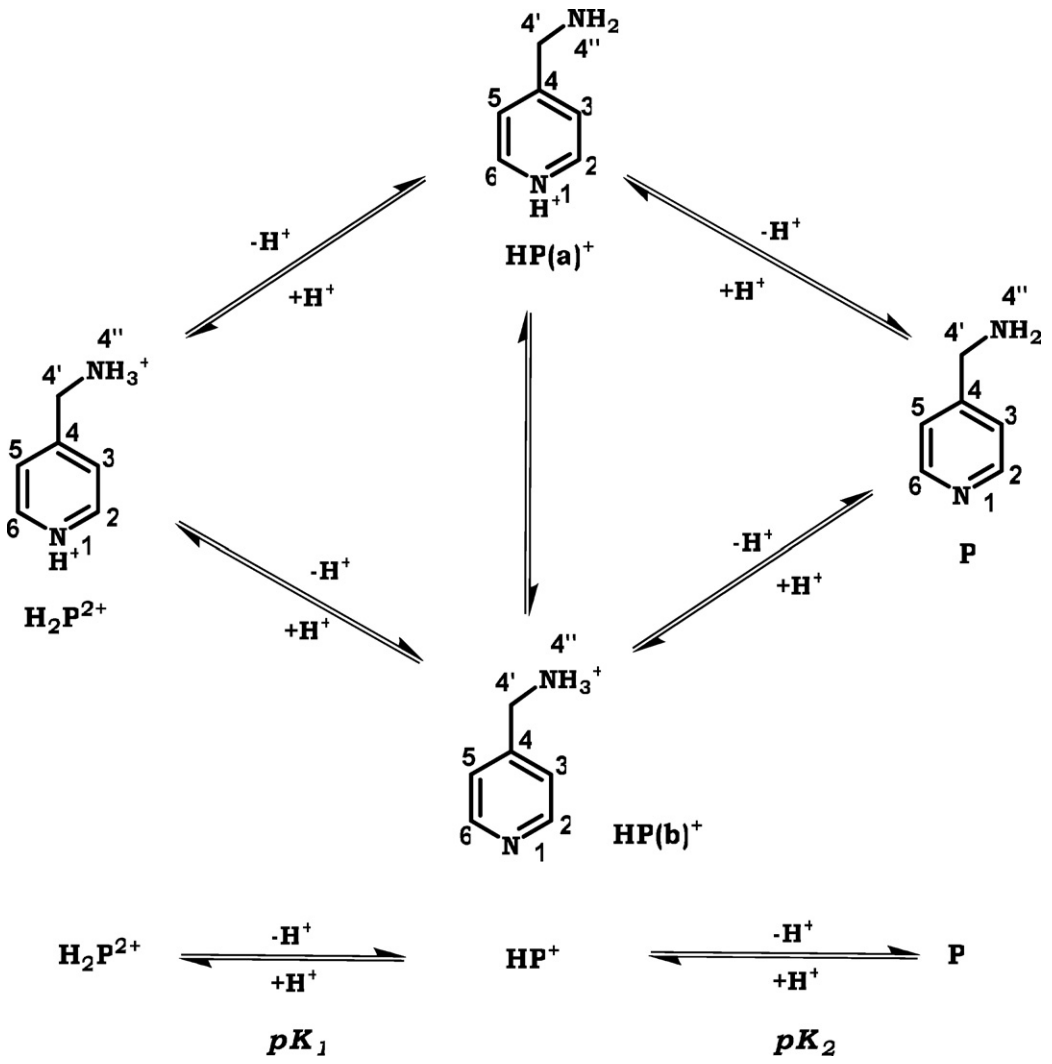

Scheme 1. Acid–base equilibria between the different forms of 4-aminomethylpyridine (4-PAM). H_2P^{2+}, HP^+ and P denote its ionic forms. HP^+ occurs as two tautomers [$HP(a)^+$ and $HP(b)^+$] in equilibrium.

lation performed on the optimized PCM-MP2/6-311++G** ground state geometry by using the random phase approximation of a time-dependent (TD) calculation [11]. The DFT exchange-correlation potentials used were the TD-Handy's functional (HCTH) [56] (TD-HCTH) and TD-B3LYP calculations in conjunction with the 6-311++G** basis set. The HCTH functional had previously been used to determine excitation energies for both small and large molecules [57,58], and B3LYP had been found to provide theoretical E_{exc} results consistent with their experimental counterparts [1,20,59]. To simulate the effects of the polar solvent the TD-DFT calculations were carried out using the PCM model. For the excited state expansion, the first 20 predicted excited states transitions were determined. The contribution of each molecular orbital transition to E_{exc} was simulated from TD Gaussian output data, using the GaussSum v. 2.1 software package [60]. All calculations were done with the software Gaussian 03 [61].

3. Results and discussion

3.1. Ground and excited state calculations

4-PAM in solution exists as three ionic forms (H_2P^{2+}, HP^+ and P) in equilibrium; in addition, the ionic form HP^+ exists as two different tautomers, namely: $HP(a)^+$, which has its N1 atom protonated and N4″ atom unprotonated, and $HP(b)^+$, where N1 is unprotonated and N4″ protonated.

Table 1 lists the most salient geometric parameters obtained in the optimization of the different molecular structures of 4-PAM + $2H_2O$ in its ground electronic state. Based on the PCM-MP2/6-311++G** results, the bond distances between N1 and its neighbouring carbon atoms (C2 and C6) are independent of the protonation status of the ionizable groups (N1 and N4″), and so are the distances between aromatic carbons. Also, protonation of N4″ considerably shortens the C4–C4′ bond and lengthens the C4–N4″ bond. On the other hand, protonation of N1 increases the C6–N1–C2 angle, whereas that of N4″ reduces the N4″–C4′–C4 angle. By contrast, the C3–C4–C5 angle does not seem to depend on the protonation status of N1 or N4″. The N4″–C4′–C4–C3 dihedral angle shows that the H_2P^{2+}, $HP(b)^+$ and P have their amino group normal to the pyridine ring.

Fig. 1 shows the canonical frontier orbitals HOMO−1, HOMO, LUMO and LUMO+1 for each 4-PAM form solvated with two water molecules. As can be seen, LUMO+1 is of the π^* type and centred on C2, C3, C5 and C6. LUMO is also a π^* orbital and spread throughout the aromatic ring. Both LUMO+1 and LUMO are identical and independent of the protonation status of the ionizable groups in all studied 4-PAM forms. This is not the case with the occupied HOMO and HOMO−1, however. Thus, when N4″ is protonated, HOMO is

Table 1
Geometric parameters for the optimized structures of $H_2P^{2+}\cdot 2H_2O$, $HP(a)^{+}\cdot 2H_2O$, $HP(b)^{+}\cdot 2H_2O$ and $P\cdot 2H_2O$ in their ground (S_0) and first two excited electronic states (S_1 and S_2).

	S_0 (Ground state)				S_1 (First excited state)[c]				S_2 (Second excited state)[c]			
	$H_2P^{2+}\cdot 2H_2O$	$HP(a)^{+}\cdot 2H_2O$	$HP(b)^{+}\cdot 2H_2O$	$P\cdot 2H_2O$	$H_2P^{2+}\cdot 2H_2O$	$HP(a)^{+}\cdot 2H_2O$	$HP(b)^{+}\cdot 2H_2O$	$P\cdot 2H_2O$	$H_2P^{2+}\cdot 2H_2O$	$HP(a)^{+}\cdot 2H_2O$	$HP(b)^{+}\cdot 2H_2O$	$P\cdot 2H_2O$
Bond lengths (Å)												
N1–C2	1.346[a]/1.330[b]	1.348[a]/1.334[b]	1.347[a]/1.323[b]	1.347[a]/1.324[b]	1.378	1.385	1.358	1.360	1.331	1.358	1.353	1.359
C2–C3	1.390[a]/1.372[b]	1.388[a]/1.367[b]	1.397[a]/1.383[b]	1.397[a]/1.383[b]	1.405	1.405	1.372	1.378	1.450	1.407	1.406	1.378
C3–C4	1.401[a]/1.389[b]	1.403[a]/1.396[b]	1.400[a]/1.386[b]	1.401[a]/1.389[b]	1.402	1.402	1.409	1.403	1.405	1.412	1.425	1.404
C4–C4′	1.507[a]/1.512[b]	1.512[a]/1.517[b]	1.504[a]/1.510[b]	1.510[a]/1.516[b]	1.499	1.510	1.498	1.513	1.503	1.521	1.495	1.513
C4′–N4″	1.495[a]/1.488[b]	1.470[a]/1.455[b]	1.498[a]/1.493[b]	1.475[a]/1.460[b]	1.493	1.458	1.505	1.467	1.492	1.462	1.503	1.467
C4–C5	1.401[a]/1.389[b]	1.401[a]/1.391[b]	1.400[a]/1.386[b]	1.401[a]/1.389[b]	1.403	1.402	1.408	1.411	1.404	1.407	1.423	1.411
C5–C6	1.390[a]/1.373[b]	1.390[a]/1.372[b]	1.398[a]/1.383[b]	1.397[a]/1.383[b]	1.404	1.405	1.373	1.373	1.449	1.404	1.403	1.373
C6–N1	1.346[a]/1.330[b]	1.346[a]/1.330[b]	1.347[a]/1.323[b]	1.347[a]/1.324[b]	1.378	1.384	1.357	1.362	1.331	1.365	1.359	1.361
Ow1–HN4″	1.670[a]/1.804[b]	–/–	1.694[a]/1.831[b]	–/–	1.809	–	1.858	–	1.816	–	1.867	–
Hw1–N4″	–/–	1.880[a]/2.066[b]	–/–	1.856[a]/2.043[b]	–	2.059	–	2.031	–	2.165	–	2.032
Ow2–HN1	1.630[a]/1.793[b]	1.654[a]/1.822[b]	–/–	–/–	1.856	1.890	–	–	1.765	1.858	–	–
Hw2–N1″	–/–	–/–	1.909[a]/2.077[b]	1.884[a]/2.049[b]	–	–	3.314	2.740	–	–	2.512	2.740
Angles (°)												
C6–N1–C2	123.0[a]/122.7[b]	122.7[a]/122.3[b]	117.6[a]/118.1[b]	117.3[a]/117.6[b]	106.3	103.7	126.2	123.2	123.9	118.6	115.3	123.4
C3–C4–C5	119.1[a]/119.5[b]	118.3[a]/118.6[b]	118.3[a]/118.3[b]	117.4[a]/117.4[b]	114.0	113.2	118.7	118.1	118.9	115.0	114.1	118.1
N4″–C4′–C4	111.2[a]/111.5[b]	113.6[a]/114.3[b]	110.9[a]/111.4[b]	113.6[a]/114.4[b]	112.4	115.0	112.4	115.3	111.9	116.0	112.6	115.3
Dihedral angles (°)												
N4″–C4′–C4–C3	−86.2[a]/−88.0[b]	−67.4[a]/−70.6[b]	−88.8[a]/−89.7[b]	−88.1[a]/−88.3[b]	−95.8	−94.8	−95.6	−97.7	−88.3	−73.1	−99.2	−97.7
N1–C2–C3–C4	0.4[a]/0.2[b]	−0.3[a]/0.0[b]	0.3[a]/0.1[b]	0.2[a]/0.1[b]	−18.8	−22.2	−11.8	−14.4	1.9	−2.7	−0.2	−1.7
C6–N1–C2–C3	0.0[a]/0.1[b]	0.1[a]/0.1[b]	0.0[a]/0.1[b]	0.0[a]/0.0[b]	48.5	52.4	38.0	43.2	-0.4	-4.5	26.1	23.3

[a] PCM-MP2/6-311++G**.
[b] PCM-HF/6-311++G**.
[c] PCM-CIS/6-311++G**.

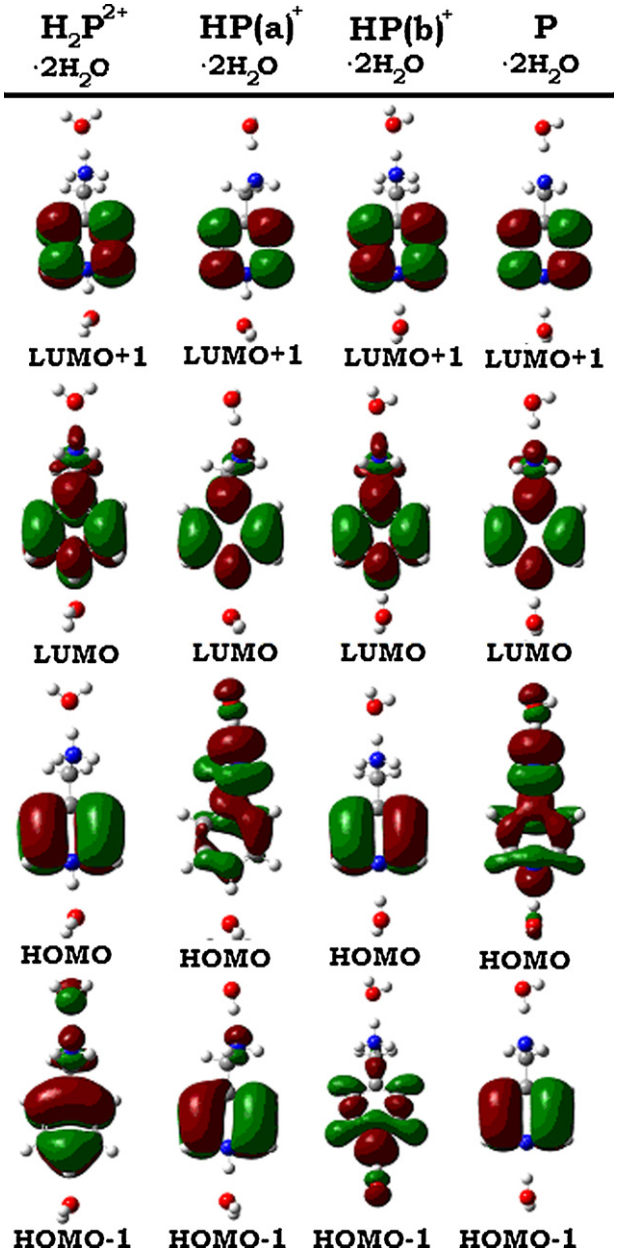

Fig. 1. Depiction of the LUMO+1, LUMO, HOMO and HOMO−1 for the species H_2P^{2+}, $HP(a)^+$, $HP(b)^+$ and P in 4-PAM with two water molecules, as obtained by using the PCM-MP2/6-311++G** method in combination with the software Gaussian cubegen. The contour interval was 0.02.

a π orbital and lies on C2, C3, C5 and C6; with N4″ unprotonated, however, HOMO is considerably different and contains a substantial contribution from the methylamino group in 4-PAM. On the other hand, deprotonation of N1 (the pyridine nitrogen) has no effect on HOMO. HOMO−1 differs in all forms, so it depends on the protonation status of both N1 and N4″. Finally, as can be seen in Fig. 1, water molecules take part in some frontier orbitals.

The theoretical calculations demonstrate that electron affinity (EA, defined as $-E_{LUMO}$) increased with increasing molecular charge: $EA(H_2P^{2+}) > EA(HP(a)^+) \approx EA(HP(b)^+) > EA(P)$. Also, deprotonation of N4″ reduced the ionization potential (IE) by *ca.* 1 eV and, somewhat more slightly, global hardness, electronegativity and electrophilicity (see supplementary material).

The geometries of the forms H_2P^{2+}, $HP(a)^+$, $HP(b)^+$ and P in their first two excited singlet states (S_1 and S_2) were optimized at the PCM-CIS/6-311++G** level. Table 1 shows the results for the most

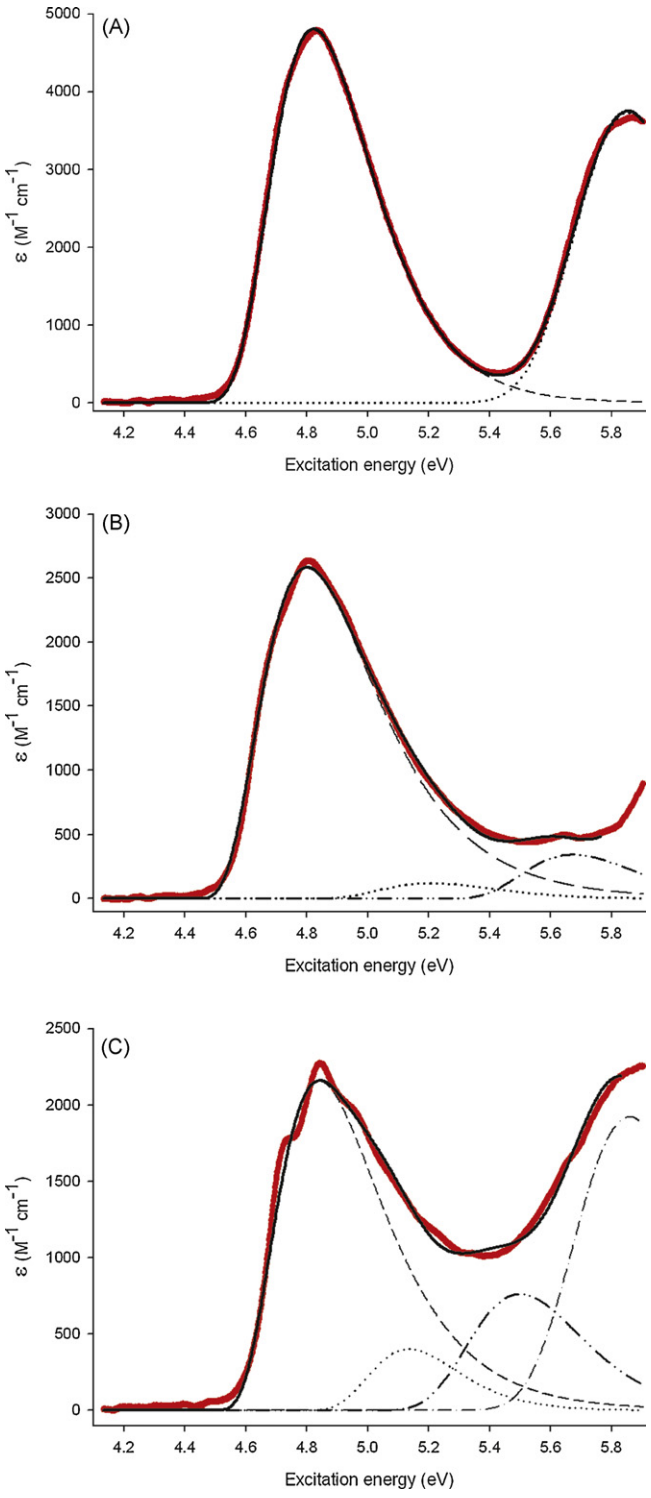

Fig. 2. Spectra for H_2P^{2+} (A), HP^+ (B) and P (C) (red lines, obtained with SPECFIT/32TM from 15 individual UV–vis spectra at pH between 1 and 13). Fitted curves (continuous line) are obtained as the combination of log-normal curves (dashed line). (For interpretation of the references to color in this figure legend, the reader is referred to the web version of the article.)

salient geometric parameters. As can be seen, the N1–C2 and N1–C6 bond lengths were longer in S_1 than in the ground state. The C2–C3 and C5–C6 bonds in the species with a protonated N1 atom [H_2P^{2+} and $HP(a)^+$] were also longer in S_1—and so were them in all forms in their S_2 state. There were no appreciable differences in C3–C4, C4–C4′ and C4–C5 bond lengths between the excited states and S_0.

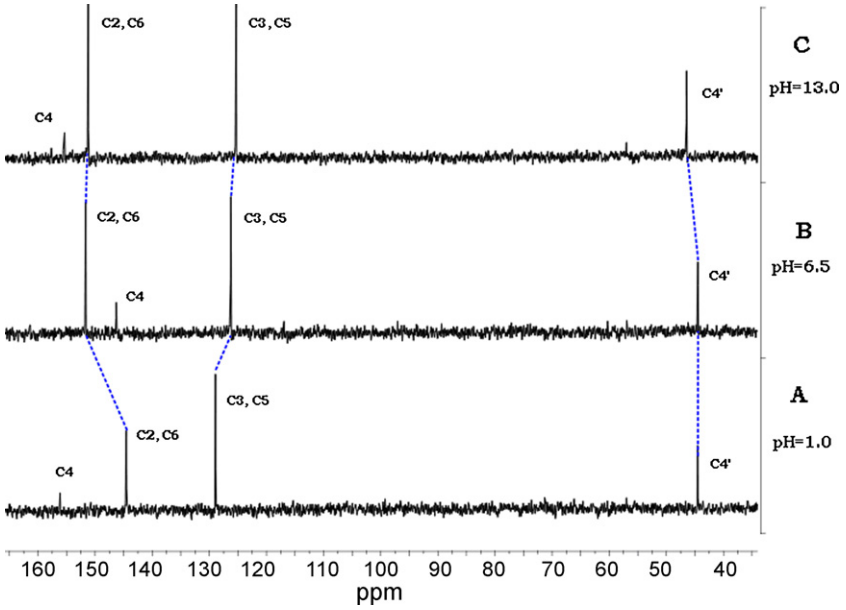

Fig. 3. ^{13}C NMR spectra for solutions containing 20 mM 4-PAM in 0.1 M HCl (A), 0.5 M phosphate buffer at pH 6.5 (B) or 0.1 M NaOH (C), all made in 80:20 H_2O-buffer/D_2O mixtures.

In the first excited state, the C6–N1–C2 angle was ~20° lower in the pyridinium species, but 7° higher in HP(b)$^+$ and P, than in S_0; this was not the case with S_2, however. Based on the N1–C2–C3–C4 and C6–N1–C2–C3 dihedral angles, the aromatic ring was distorted by effect of electronic excitation. Thus, in S_1 the ring was less planar than in S_0 and adopted a semi-chair conformation at N1 in all studied forms. In S_2, however, only the species with a deprotonated N1 atom exhibited this change. The previous results are consistent with experimental values reported by Baba et al. [62] and theoretical calculations of Cai and Reimers [30], who showed pyridine in its first excited state to loss some planarity and adopt a boat conformation. Our results show that methylation at C4 hinders geometric distortion in the molecule and allows it to adopt a semi-chair conformation at most. Also, the N4″–C4′–C4–C3 dihedral angles show that all 4-PAM forms have their amino group normal to the pyridine ring in S_1. The electronic excitation also decreases the strength of the hydrogen bond formed between the pyridinic N1 and the water molecule proton.

3.2. Theoretical and experimental study of the excitation energies of 4-PAM molecular forms

The experimental absorption spectra for aqueous 4-PAM solutions at pH 1–13 were fitted to the ionic equilibrium of Scheme 1 by using the software SPECFIT/32^{TM} [47]. This allowed the characteristic UV–vis spectrum for each ionic form to be obtained (Fig. 2) and its macroscopic ionization constants at 25 °C at I = 0.1 M calculated. The resulting constants (pK_1 = 4.0 ± 0.1 and pK_2 = 8.4 ± 0.1) were slightly lower than those obtained by potentiometric titration of 4-PAM in D_2O at 25 °C by Crugeiras et al. [44].

The UV–vis spectrum for each ionic form of 4-PAM was deconvoluted into individual bands, using the software PeakFit v. 4.0 [52]. As in previous works, the number of variables to be optimized was minimized by using $W = 3.5 \times 10^3$ cm^{-1} for the bands with $E_{exc} > 5.1$ eV; the corresponding value for the electronic transitions with $E_{exc} < 5.1$ eV was 2.8×10^3 cm$^{-1} \leq W \leq 3.4 \times 10^3$ cm^{-1} [37–43,49–51]. The bands with $E_{exc} > 5.1$ eV were assumed to have $\rho = 1.4$. Table 2 lists the excitation energy, the band width, asymmetry, area and intensity (ε) obtained from the fitting. The experimental f values were calculated from the following equation [63]:

$$f = 4.32 \times 10^{-9}\, \Delta\nu_{1/2} \varepsilon^{\lambda\,max}$$

where $\varepsilon^{\lambda max}$ is the molar absorption coefficient at the band peak and $\Delta\nu_{1/2}$ the band width at half $\varepsilon^{\lambda max}$.

The UV–vis spectrum for the species H_2P^{2+} was deconvoluted into two log–normal bands (Fig. 2A). Band I, centred at 4.82 eV, corresponded to the first π–π* transition and peaked at an energy value similar to that for pyridinium ion (4.87 eV [37]). Band II, centred at 5.8 eV, spanned energy values within the reported range for the second π–π* transition for pyridine derivatives [37].

The energies of the first 20 electronic excitations in each 4-PAM form were calculated by using the PCM-TD-DFT method in conjunction with the HCTH and B3LYP functionals and 6-311++G** basis sets (see Section 2.1). Table 3 shows the excitation energies (E_{exc}), the corresponding oscillator strengths (f) and the orbital transition most strongly contributing to the excitation. As can be seen, the B3LYP energies exceeded the HCTH values, which is consistent with previously reported data [64,65].

As can be seen in Table 3, both methods predict two electron transitions for H_2P^{2+}. The experimental E_{exc} value for the first transition was *ca.* 0.4 eV lower than those calculated with the B3LYP functional and *ca.* 0.3 eV lower than those provided by the HCTH functional. Additionally, the electronic excitation energies of the two transitions predicted by HCTH functional are quite close to the experimental values. Therefore, the latter method reproduces the electronic spectrum better than B3LYP does.

Fig. 2B shows the UV–vis spectrum for the ionic species HP$^+$, which occurs as two tautomers [HP(a)$^+$ and HP(b)$^+$] in equilibrium. Unequivocally assigning the electronic transitions established from the deconvoluted spectra to each tautomer requires a quantitative knowledge of the tautomeric equilibrium. Fig. 3 shows the ^{13}C NMR spectra for 4-PAM at pH 1.0, 6.5 and 13.0, where H_2P^{2+}, HP$^+$ and P, respectively, were the major forms. The spectrum obtained at pH 6.5 (HP$^+$ species) was consistent with the presence of a single tautomer rather than a mixture of them. The shifts in the signals for the C2, C3, C5 and C6 observed at this pH were identical to that obtained at pH 13.0 and rather different from those obtained at pH 1.0. This fact clearly shows that at pH 6.5 and 13.0 the pyridine nitrogen has

Table 2
Excitation energies values, molar absorption coefficients, band width, asymmetry and molar area for the log–normal bands used in deconvolution processes done on each 4-PAM ionic form.

Band		H_2P^{2+}	HP^+	P
Band I	E_{exc} (eV)	4.82 ± 0.01	4.82 ± 0.01	4.84 ± 0.01
	ε (M^{-1} cm^{-1})	4804 ± 4	2533 ± 3	2156 ± 8
	Band width $\times10^{-3}$ (cm^{-1})	3.21 ± 0.01	3.69 ± 0.03	3.4[a]
	Asymmetry (ρ)	1.49 ± 0.01	1.67 ± 0.01	1.65[a]
	Area (km mol^{-1})	169.3 ± 8.5	104.9 ± 0.8	82.0 ± 4.1
Band II	E_{exc} (eV)	5.8[b]	5.20 ± 0.01	5.10 ± 0.08
	ε (M^{-1} cm^{-1})	3750[b]	151 ± 21	314 ± 14
	Band width $\times10^{-3}$ (cm^{-1})	3.5[a]	3.5[a]	2.8[a]
	Asymmetry (ρ)	1.17[b]	1.4[a]	1.4[a]
	Area (km mol^{-1})	140[b]	5.7 ± 0.1	9.5 ± 0.5
Band III	E_{exc} (eV)	–	5.6[b]	5.39 ± 0.09
	ε (M^{-1} cm^{-1})	–	230[b]	558 ± 15
	Band width $\times10^{-3}$ (cm^{-1})	–	3.5[a]	3.5[a]
	Asymmetry (ρ)	–	1.4[a]	1.4[a]
	Area (km mol^{-1})	–	8.7[b]	21.2 ± 1.0
Band IV	E_{exc} (eV)	–	–	5.7[b]
	ε (M^{-1} cm^{-1})	–	–	1900[b]
	Band width $\times10^{-3}$ (cm^{-1})	–	–	3.5[a]
	Asymmetry (ρ)	–	–	1.4[a]
	Area (km mol^{-1})	–	–	75[b]

[a] Values fixed in the fitting process.
[b] The absence of experimental values for the zone of the band peak lead us to assume a large experimental error in the band values.

Table 3
Comparison of the theoretical and experimental electronic excitation energies (E_{exc}) and oscillator strengths (f) for the different forms of 4-PAM solvated with two water molecules. Only those theoretical transitions with f > 0.005 over the E_{exc} range 2.6–6.2 eV were considered.

	HCTH/6-311++G**			B3LYP/6-311++G**			Experimental	
	[a]E_{exc}	[b]f	[c]T	[a]E_{exc}	[b]f	[c]T	[a]E_{exc}	[b]f
$H_2P^{2+}\cdot2H_2O$	5.161	0.085	H → L (70%)	5.267	0.112	H → L (77%)	4.82	0.07
	5.943	0.029	H−3 → L (54%)	6.038	0.038	H-1 → L (78%)	5.8	–
$HP(a)^+\cdot2H_2O$	3.470	0.070	H → L (94%)	4.351	0.082	H → L (95%)	–	–
	4.097	0.009	H → L+1(98%)	5.122	0.009	H → L+1 (87%)	–	–
	5.282	0.078	H−2 → L (70%)	5.435	0.108	H−2 → L (65%)	–	–
$HP(b)^+\cdot2H_2O$	5.112	0.055	H−2 → L (71%)	5.260	0.053	H → L (76%)	4.82	0.04
	5.493	0.018	H−4 → L (88%)				5.6	–
$P\cdot2H_2O$	4.282	0.081	H → L (94%)	4.973	0.046	H → L (67%)	4.84	0.03
	4.791	0.022	H−1 → L (91%)	5.281	0.028	H−1 → L (52%)	5.10	0.01
	5.260	0.048	H−3 → L (59%)	5.374	0.091	H−2 → L (61%)	5.39	0.01
	5.738	0.034	H → L+3 (96%)	5.455	0.020	H−2 → L+1 (55%)	5.7	–

[a] E_{exc} appears in eV.
[b] f represents the oscillator strength value.
[c] T represents the main orbital transition contribution to excitation.

the same protonation state (deprotonated). By contrast, the shift in the signal for C4′ was essentially the same at pH 1.0 and 6.5, showing that the methylamino group presents the same protonation state (protonated). These results clearly show that the tautomeric equilibrium is strongly displaced to $HP(b)^+$, which account for virtually the whole ionic form HP^+. ^{13}C NMR spectra for pyridine and benzylamine (see supplementary material) demonstrate that the C4 signal is affected by the protonation of both N1 and N4″, for this reason this signal should not be used to determine the nitrogen protonation state.

The UV–vis spectrum for the ionic species HP^+, which was assigned to $HP(b)^+$, was deconvoluted into three log–normal curves. The band parameters obtained are given in Table 2. Band I, centred at 4.82 eV, had the same E_{exc} value as the first π–π* transition in the species H_2P^{2+}. This confirms that deprotonation of N1 has virtually no effect on the electronic excitation energy of 4-PAM and is consistent with the deprotonation results obtained for other pyridine compounds such as 4-methylpyridine and pyridine itself (results not shown). Thus, the increase in E_{exc} for the first π–π* transition in pyridoxamine with a deprotonated pyridine nitrogen (*ca.* 0.18 eV [38]) cannot be exclusively due to the effect of the pyridine nitrogen. Band II, centred at 5.20 eV, was a submerged band (*i.e.* one with the small ε value) included in the study to improve the fitting. Submerged bands have been widely used to deconvolute UV–vis spectra with a view to fitting spectral valleys [37–43,49–51]. Band III was centred at 5.6 eV and due to the second π–π* transition. As can be seen from Table 3, the experimental excitation energies for bands I and III were closer to the theoretical HCTH values than to the B3LYP values, since the last one just predicts just one transition.

As can be seen in Table 2 (and also in Fig. 2A and B) the protonation of pyridinic N1 has no effect on the E_{exc} of band I. By contrast the protonation has remarkable effect on the band intensity, reflected on the molar absorption coefficient (4804 M^{-1} cm^{-1} in H_2P^{2+} and 2533 M^{-1} cm^{-1} in $HP(b)^+$) and the oscillator strength (0.07 in H_2P^{2+} and 0.04 in $HP(b)^+$, see Table 3). Theoretical calculations predict similar trend, both HCTH and B3LYP functional predict identical E_{exc} values and a remarkable decrease in the f value of $HP(b)^+$ with regard to H_2P^{2+}.

Fig. 2C shows the UV–vis spectrum for the species P, which, similarly to the neutral forms of pyridine, 4-methylpyridine (results not

shown), benzene and toluene, exhibits the vibrational fine structure [58]. Band I, centred at 4.84 eV and assigned to a π–π^* transition, had a 0.02 eV higher energy than the first transition for the species H_2P^{2+} and $HP(b)^+$. Such a slight increase is similar to that observed by effect of the deprotonation of the amino group in pyridoxamine (*ca.* 0.03 eV [38]). Band II, which was centred at 5.10 eV and buried under the curve for the first transition, was assigned to an n–π^* transition [37], however, the TD-DFT calculations assign this band to an H-1 → L transition, which is a π–π^* transition. The band centred at 5.39 eV was a submerged band, whereas that at 5.7 eV corresponded to other π–π^* transition.

Deprotonation of both N1 and N4″ were reflected on the increase of band number, due to the increase of n–π^* transitions. Similar trend was predicted by theoretical calculations, both functionals predict four electronic transitions (the same number that experimentally obtained). Additionally, E_{exc} values provided by the B3LYP functional were highly similar to the experimental ones.

The HCTH functional provides good predictions of the experimental excitation energies for the cationic and dicationic species (H_2P^{2+} and $HP(b)^+$), whereas the B3LYP functional affords good simulation of the electronic transitions for the neutral species (P). The same trend has been observed in similar compounds (results not shown).

Results obtained in this work clearly show that the transition number and the energy of these transitions provided by the TD-DFT method are quite consistent with their experimental values. Therefore, the results of TD-DFT computations with the right functional can be used to study and rationalize electronic transitions.

Acknowledgements

This work was funded by Spain's Government via Project CTQ-2008-02207/BQU). The authors are also grateful to the Supercomputational Centre of Catalonia (CESCA) for access to its computing facilities.

Appendix A. Supplementary data

Supplementary data associated with this article can be found, in the online version, at doi:10.1016/j.jphotochem.2009.10.003.

References

[1] M. Altarsha, G. Monrad, B. Castro, J. Mol. Struct. (Theochem) 761 (2006) 203–207.
[2] S.P. Kwasniewski, M.S. Deleuze, J.P. François, Int. J. Quantum Chem. 80 (2000) 672–680.
[3] G.R. Hutchison, M.A. Ratner, T.J. Marks, J. Phys. Chem. A 106 (2002) 10596–10605.
[4] M.T. Cash, P.R. Schreiner, R.S. Phillips, Org. Biomol. Chem. 3 (2005) 3701–3706.
[5] M. Sun, Chem. Phys. 320 (2006) 155–163.
[6] R. Andreu, J. Garín, J. Orduna, Tetrahedron 57 (2001) 7883–7892.
[7] S. Fantacci, A. Migani, M. Olivucci, J. Phys. Chem. A 108 (2004) 1208–1213.
[8] J. Finley, P.-A. Malmqvist, B.O. Roos, L. Serrano-Andrés, Chem. Phys. Lett. 288 (1998) 299–306.
[9] R. Crespo, M. Merchán, J. Michl, J. Phys. Chem. A 104 (2000) 8593–8599.
[10] T. Korona, H.-J. Werner, J. Chem. Phys. 118 (2003) 3006–3019.
[11] R.E. Stratmann, G.E. Scuseria, J. Chem. Phys. 109 (1998) 8218–8224.
[12] B.D. Slaughter, M.W. Allen, G.H. Lushington, C.K. Johnson, J. Phys. Chem. A 107 (2003) 5670–5680.
[13] R.J. Deeth, Faraday Discuss 124 (2003) 379–391.
[14] F. De Angelis, S. Fantacci, A. Sgamellotti, M. Pizzotti, F. Tessore, A.O. Biroli, Chem. Phys. Lett. 447 (2007) 10–15.
[15] S.J.A. Gisbergen, J.G. Snijders, E.J. Baerends, Phys. Rev. Lett. 78 (1997) 3097–3100.
[16] D. Jacquemin, E.A. Perpète, X. Assfeld, G. Scalmani, M.J. Frisch, C. Adamo, Chem. Phys. Lett. 438 (2007) 208–212.
[17] A.L. Sobolewski, W. Domcke, C. Dedonder-Lardeux, C. Jouvet, Phys. Chem. Chem. Phys. 4 (2002) 1093–1100.
[18] C. Dedonder-Lardeux, C. Jouvet, S. Perun, A. Sobolewski, Phys. Chem. Chem. Phys. 5 (2003) 5118–5126.
[19] E.J. Baerends, G. Ricciardi, A. Rosa, S.J.A. van Gisbergen, Coord. Chem. Rev. 438 (2007) 208–212.
[20] J. Preat, D. Jacquemin, E.A. Perpète, Chem. Phys. Lett. 415 (2005) 20–24.
[21] Z. Huang, Z. Lin, C. Song, J. Phys. Chem. A 111 (2007) 4340–4352.
[22] D.M. Rogers, N.A. Besley, P. O'Shea, J.D. Hirst, J. Phys. Chem. B 109 (2005) 23061–23069.
[23] T. Andruniow, P.M. Kozlowski, M.Z. Zgierski, J. Chem. Phys. 115 (2001) 7522–7533.
[24] M.K. Shukla, J. Leszczynski, J. Comput. Chem. 25 (2004) 768–778.
[25] I. Antol, M. Eckert-Maksic, M. Klessinger, J. Mol. Struct. (Theochem) 664–665 (2003) 309–317.
[26] S. Jang, S.I. Jin, C. Ryang Park, Bull. Korean Chem. Soc. 28 (2007) 2343–2353.
[27] L. Zhang, G.H. Peslherbe, J.M. Muchall, Photochem. Photobiol. 82 (2006) 324–331.
[28] J. Gao, N. Li, M. Freindorf, J. Am. Chem. Soc. 118 (1996) 4912–4913.
[29] Z.-L. Cai, J.R. Reimers, J. Phys. Chem. A 104 (2000) 8389–8408.
[30] Z.-L. Cai, J.R. Reimers, J. Phys. Chem. A 106 (2002) 8769–8778.
[31] J. Lorenc, E. Kucharska, J. Hanuza, H. Chojnacki, J. Mol. Struct. 707 (2004) 47–57.
[32] J. Lorenc, J. Mol. Struct. 748 (2005) 91–100.
[33] M.L. Dell'Arciprete, C.J. Cobos, J.P. Furlong, D.O. Mártire, M.C. González, Chem. Phys. Chem. 8 (2007) 2498–2505.
[34] I. Díaz, L.A. Montero, F. Muñoz, J. Donoso, J. Mol. Struct. (Theochem) 433 (1998) 279–290.
[35] J.N. Jansonius, Curr. Opin. Struct. Biol. 8 (1998) 759–769.
[36] P.A. Voziyan, B.G. Hudson, Cell. Mol. Life Sci. 62 (2005) 1671–1681.
[37] D.E. Metzler, C.M. Harris, R.J. Johnson, D.B. Siano, J.A. Thompson, Biochemistry 12 (1973) 5377–5392.
[38] B. Vilanova, M. Adrover, F. Muñoz, J. Donoso, Chem. Biodiver. 1 (2004) 1073–1090.
[39] C.M. Harris, R.J. Johnson, D.E. Metzler, Biochim. Biophys. Acta 421 (1976) 181–194.
[40] J.M. Sánchez-Ruiz, J. Llor, E. López-Cantarero, M. Cortijo, An. Quim. 80 (1984) 708–714.
[41] M.A. Vázquez, F. Muñoz, J. Donoso, F. García-Blanco, J. Chem. Soc. Perkin Trans. II (1991) 275–281.
[42] M.A. Vázquez, F. Muñoz, J. Donoso, F. García-Blanco, Biochem. J. 279 (1991) 759–767.
[43] J. Donoso, F. Muñoz, F. García-Blanco, Biochem. J. 292 (1993) 225–229.
[44] J. Crugeiras, A. Rios, T.L. Amyes, J.P. Richard, Org. Biomol. Chem. 3 (2005) 2145–2149.
[45] P.A. Voziyan, R.G. Khalifah, C. Thibaudeau, A. Yildiz, J. Jacob, A.S. Serianni, B.G. Hudson, J. Biol. Chem. 278 (2003) 46616–46624.
[46] M. Adrover, B. Vilanova, J. Frau, F. Muñoz, J. Donoso, J. Bioorg. Med. Chem. 16 (2008) 5557–5569.
[47] R.A. Binstead, A.D. Zuberbühler, B. Jung, SPECFIT/32, v 3.0.23, Spectrum Software Associates©, 1993–2001.
[48] D.B. Siano, D.E. Metzler, J. Chem. Phys. 51 (1969) 1856–1861.
[49] C.M. Metzler, A.E. Cahill, S. Petty, D.E. Metzler, L. Lang, Appl. Spectrosc. 39 (1985) 333–339.
[50] C.M. Metzler, A. Cahill, D.E. Metzler, J. Am. Chem. Soc. 102 (1980) 6075–6082.
[51] C.M. Metzler, D.E. Metzler, Anal. Biochem. 166 (1987) 313–327.
[52] PeakFit v. 4.0, AISN Software, Erkrath, Germany, 1995.
[53] M. Head-Gordon, J.A. Pople, M.J. Frisch, Chem. Phys. Lett. 153 (1988) 503–506.
[54] J.B. Foresman, M. Head-Gordon, J.A. Pople, J. Phys. Chem. 96 (1992) 135–149.
[55] J. Tomasi, M. Persico, Chem. Rev. 94 (1994) 2027–2094.
[56] F.A. Hamprecht, A.J. Cohen, D.J. Tozer, N.C. Handy, J. Chem. Phys. 109 (1998) 6264–6271.
[57] E. San Fabián, L. Pastor-Abia, Theor. Chem. Account 118 (2007) 637–642.
[58] T. Yanai, R.J. Harrison, N.C. Handy, Mol. Phys. 103 (2005) 413–424.
[59] M.K. Shukla, J. Leszczynski, J. Phys. Chem. A 107 (2003) 5538–5543.
[60] N.M. O'Boyle, A.L. Tenderholt, K.M. Langer, J. Comp. Chem. 29 (2008) 839–845.
[61] M.J. Frisch, G.W. Trucks, H.B. Schlegel, G.E. Scuseria, M.A. Robb, J.R. Cheeseman, J.A. Montgomery Jr., T. Vreven, K.N. Kudin, J.C. Burant, J.M. Millam, S.S. Iyengar, J. Tomasi, V. Barone, B. Mennucci, M. Cossi, G. Scalmani, N. Rega, G.A. Petersson, H. Nakatsuji, M. Hada, M. Ehara, K. Toyota, R. Fukuda, J. Hasegawa, M. Ishida, T. Nakajima, Y. Honda, O. Kitao, H. Nakai, M. Klene, X. Li, J.E. Knox, H.P. Hratchian, J.B. Cross, V. Bakken, C. Adamo, J. Jaramillo, R. Gomperts, R.E. Stratmann, O. Yazyev, A.J. Austin, R. Cammi, C. Pomelli, J.W. Ochterski, P.Y. Ayala, K. Morokuma, G.A. Voth, P. Salvador, J.J. Dannenberg, V.G. Zakrzewski, S. Dapprich, A.D. Daniels, M.C. Strain, O. Farkas, D.K. Malick, A.D. Rabuck, K. Raghavachari, J.B. Foresman, J.V. Ortiz, Q. Cui, A.G. Baboul, S. Clifford, J. Cioslowski, B.B. Stefanov, G. Liu, A. Liashenko, P. Piskorz, I. Komaromi, R.L. Martin, D.J. Fox, T. Keith, M.A. Al-Laham, C.Y. Peng, A. Nanayakkara, M. Challacombe, P.M.W. Gill, B. Johnson, W. Chen, M.W. Wong, C. Gonzalez, J.A. Pople, Gaussian 03, Revision C. 02, Gaussian, Inc., Wallingford CT, 2004.
[62] H. Baba, L. Goodman, P.C. Valenti, J. Am. Chem. Soc. 88 (1966) 5410–5415.
[63] V.B. Bojinov, I.P. Panova, Dyes Pigments 74 (2007) 551–560.
[64] C. Adamo, G.E. Scuseria, V. Barone, J. Chem. Phys. 111 (1999) 2889–2899.
[65] Y. Shigemitsu, K. Komiya, N. Mizuyama, Y. Tominaga, J. Mol. Struct. (Theochem) 855 (2008) 92–101.